ORIGINAL ARTICLE



AutoInFocus, a new paradigm for ultrasound-guided spine intervention: a multi-platform validation study

Keshuai Xu¹ → Baichuan Jiang¹ · Abhay Moghekar² · Peter Kazanzides¹ · Emad Boctor¹

Received: 28 January 2022 / Accepted: 23 February 2022 / Published online: 25 March 2022 © CARS 2022

Abstract

Purpose: Ultrasound-guided spine interventions often suffer from the insufficient visualization of key anatomical structures due to the complex shapes of the self-shadowing vertebrae. Therefore, we propose an ultrasound imaging paradigm, AutoInFocus (automatic insonification optimization with controlled ultrasound), to improve the key structure visibility.

Methods: A phased-array probe is used in conjunction with a motion platform to image a controlled workspace, and the resulting images from multiple insonification angles are combined to reveal the target anatomy. This idea is first evaluated in simulation and then realized as a robotic platform and a miniaturized patch device. A spine phantom (CIRS) and its CT scan were used in the evaluation experiments to quantitatively and qualitatively analyze the advantages of the proposed method over the traditional approach.

Results: We showed in simulation that the proposed system setup increased the visibility of interspinous space boundary, a key feature for lumbar puncture guidance, from 44.13 to 67.73% on average, and the 3D spine surface coverage from 14.31 to 35.87%, compared to traditional imaging setup. We also demonstrated the feasibility of both robotic and patch-based realizations in a spine phantom study.

Conclusion: This work lays the foundation for a new imaging paradigm that leverages redundant and controlled insonification to allow for imaging optimization of the complex vertebrae anatomy, making it possible for high-quality visualization of key anatomies during ultrasound-guided spine interventions.

Keywords Ultrasound imaging · Image-guided procedure · Spine intervention · Medical robotics

Introduction

Extensive research has been conducted with ultrasound imaging to guide spinal interventions [1–5]. However, they often suffer from suboptimal insonification of key anatomical structures due to the complex shapes of the self-shadowing vertebrae, which complicates the image interpretation and reduces the success rate [1]. This challenge is especially

Keshuai Xu and Baichuan Jiang have been contributed equally to this work

> Keshuai Xu keshuai@jhu.edu

- Department of Computer Science, Johns Hopkins University, Baltimore 21218, MD, USA
- Department of Neurology, The Johns Hopkins University School of Medicine, Baltimore 21205, MD, USA

highlighted in ultrasound-guided lumbar puncture [5,6], a common procedure to collect cerebrospinal fluid (CSF) using a needle inserted through a gap between the spinous processes on the vertebrae. This critical feature is poorly visualized for needle insertion guidance due to the shadowing artifacts and combined with other risk factors such as obesity [7] and spine anomalies [8], can lead to failures and repeated attempts, which increase the risk of complications including CSF leak and headache [9]. Additionally, traumatic lumbar punctures result in blood contamination of CSF, which confuses diagnostics [10] and introduces infections [11].

Several approaches have been proposed to address this issue and provide better guidance. In [2], the authors took a registration-based approach that tries to register the intra-operative ultrasound with statistical shape models of the spine for enhanced guidance. However, when targeting patients with severe spine malformations or pediatric patients, the atlas-based registration approach may not deliver. Similarly, a commercial hand-held ultrasound



machine Rivanna Accuro uses image recognition to assist in marking the needle insertion site for epidural placements. It provides real-time guidance through a needle guide for paramedian epidurals but is incompatible with the median approach of lumbar puncture because the probe covers the needle insertion site. Also, holding the probe during needle insertion is not recommended due to the loss of ability to use both hands for needle insertion, stabilization, and depth control [12]. Another approach is to integrate an ultrasound element in the needle tip [3,4,13,14], which can provide needle insertion guidance from inside to navigate through anatomy. While the latter approaches have the advantage of being registration-free, they either provide limited guidance information with non-imaging modalities or require a sweeping motion of the needle to form an image, which is sometimes impractical when the needle is in deeper tissues or close to vital structures.

In this work, we propose an ultrasound imaging paradigm AutoInFocus (automatic insonification optimization with controlled ultrasound) to improve the image guidance for spinal interventions. We hypothesize that using redundant (imaging the same anatomical area from multiple angles) and controlled (driven by motion platforms instead of freehand) insonification, the complex and critical structures of the spine, such as interspinous space during lumbar puncture, can be detected with high clarity. Besides, imaging optimization can be achieved by identifying critical insonification windows with image-based approaches and controlling ultrasound beam steering toward these windows to adaptively image the key anatomy. The required precise motion is not easily accomplished by a human hand holding a tracked probe and thus motivates a robotic approach. To summarize, the AutoInFocus paradigm contains the following key elements:

- A phased array probe is utilized instead of a traditional linear array due to the superior beam steering ability and smaller form factor for easier skin coupling and avoiding interference with the needle.
- 2. A controlled transducer motion workspace to allow viewing the anatomy from different insonification windows on the patient's surface.
- 3. A mechanical deployment of the designed motion workspace suitable for the target clinical scenarios.
- 4. An optimization approach for enhancing visualization of key anatomical structures under the controlled workspace.

In the following sections, we will introduce three different platforms for validating a specific AutoInFocus setup and demonstrate that it can give us superior visibility of the complex shaped lumbar bone anatomy. In this work, we focused on platform development and validation, and advanced image-based optimization algorithms will be introduced in future work.



Fig. 1 The proposed 2 DOF motion of the transducer (orange cylinder). We scan the spine paramedianally with a phased array transducer that mechanically translates (green arrows) and rotates (magenta arrow). Our experiment setups further tilt the transducer toward the midline

Methodology

Following the AutoInFocus paradigm, we configured our validation experiments with the following elements:

- 1. An ATL P7-4 phased array probe.
- A two-degree-of-freedom (DOF) motion workspace with 1-DOF translation and 1-DOF rotation, as shown in Fig. 1. The translational axis is placed parallel to the spine midline with a lateral offset that exposes the midline for needle insertion.
- A robot arm (Universal Robots UR3) platform for spine surgeries and a wearable patch device for lumbar puncture deployment.
- A simple distance-based compounding to combine all insonification angle images for highlighting the key anatomy.

To investigate the feasibility and benefit of this setup for spinal intervention guidance, we developed three validation platforms. First, ultrasound simulation was used to analyze the theoretical effectiveness. Then, we developed a robotic version and a miniaturized patch device version as two realizations for further validation.

Ultrasound simulation-based validation platform

Before going into the hardware development, we evaluated the performance of AutoInFocus in simulation. Extensive research has been done in the field of ultrasound simulation. Traditionally, algorithms are based on wave-front propagation in tissue, simulating the system's spatial impulse response and convolving with a predefined micro-scatter map. This approach can render the highest realism and is well-established in software packages such as Field-II [15] and K-wave [16]. However, they are too computationally expensive to handle our workload of hundreds of B-mode images per scan. Therefore, we used the convolutional ray-tracing-based fast ultrasound simulation technique proposed by Mehrdata *et al.* [17] (ImFusion software). It is well-suited because realistic US imaging artifacts, e.g., shadowing, can



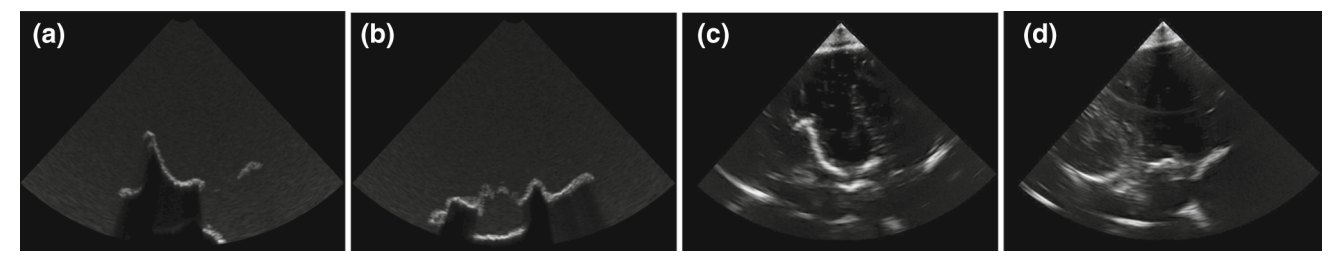


Fig. 2 Comparison of simulated and real ultrasound images of a spine phantom. a-b Simulated B-mode images from a CT scan of the phantom. c-d Respective real B-mode images from the real phantom

be generated by ray optics, which is sufficient for analyzing the effectiveness of the proposed methods.

The convolutional ray-tracing US simulator contains two major parts: (1) ray optics and (2) scattering convolution. These two parts require a medium map to be generated for the simulation target beforehand, where each medium is associated with acoustic parameters such as speed of sound value, attenuation coefficient, and acoustic impedance. These acoustic parameters are used in the ray-tracing engine, while another set of scatterer density coefficients is used during scattering convolution [18]. For obtaining a medium map as the simulation input, we have acquired a CT scan of a lumbar spine phantom (Fig. 3) and manually segmented the spine by thresholding and smoothing operations. The spine was assigned with bone acoustic properties and the background medium is simulated as soft tissue with minimum speckle noise.

By defining a phased array geometry and a pose on the medium map, a 2D ultrasound image can be simulated as output. As a qualitative validation, sample images of the simulation are presented in Fig. 2. The boundaries of the spine are highlighted, with shadow artifacts present in both simulated images and real ultrasound images of the same spine model.

Robot-based validation platform

One realization of AutoInFocus is achieved by using a robot arm (Universal Robots UR3) to hold a phased array probe (ATL P7-4), targeting the spinal surgery scenarios. Then the designed AutoInFocus workspace can be reached with high dexterity and accuracy using the 6-DOF robot. The overall robotic setup is shown in Fig. 3. Two optical markers on the transducer holder were tracked by an external optical tracker (Atracsys FusionTrack500) to maximize the marker visibility for extreme poses during system calibration.

We calibrated the system in two steps: First, the TXp calibration for identifying marker-to-ultrasound transformation X_1 and then the AXXB calibration for robot-to-marker transformation X_2 .

Marker-to-ultrasound calibration

We first carry out the TXp cross-wire calibration experiment (Fig. 3a) to identify X_1 . The calibration steps are the following:

- Compute relative transformation between the two markers
- Calibrate for the temporal offset between the tracking timestamp and image timestamp. The two data streams are synchronized via a sinusoidal motion matching. After calibration, the average temporal error is 14.23 ms.
- 3. Image the cross-wire phantom from multiple probe poses B_i and annotate the cross-wire point location p_i in the image.
- 4. Solve a system of equations $T_i * X_1 * p_i = const$ for X_1 with a gradient descent approach [19,20].

In total, N=251 data frames were collected. Using the computed calibration matrix X_1 , the cross-wire point reprojection error has a standard deviation of 1.84 mm, 0.45 mm, 0.88 mm in the x, y, z directions, respectively.

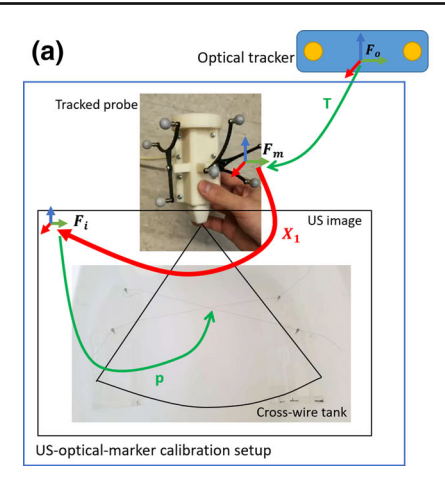
Robot-to-marker calibration

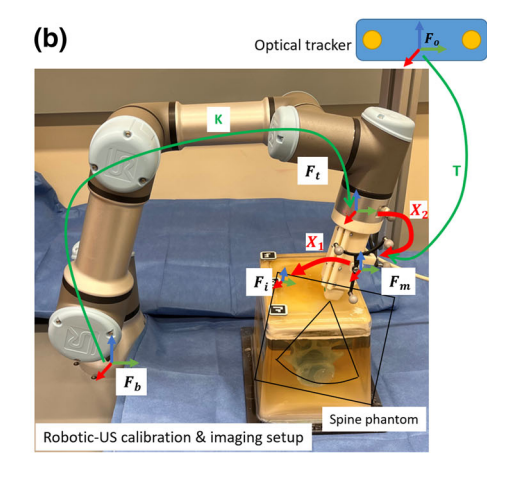
An AXXB hand-eye calibration (Fig. 3b) is performed to identify the robot-to-marker transformation X_2 , via the following steps:

- 1. After mounting the ultrasound probe to the UR3 robot, the robot was moved to various poses, for which the tool tip poses K_i from the robot kinematics and the marker poses T_i from the optical tracker were recorded.
- 2. For two robot poses i, j, we can establish an equation of $A_{ij} * X_2 = X_2 * B_{ij}$ from the transformation chain, where $A_{ij} = K_i^{-1} * K_j$ and $B_{ij} = T_i^{-1} * T_j$ are the relative motion matrices. With varying poses of the robot, a set of equations in the form AX = XB can be established.
- 3. The system of AX = XB equations can be solved with methods introduced in [21], and transformation X_2 can be computed.



Fig. 3 Robotic evaluation platform. **a** US-optical-marker TXp calibration setup. **b** Robot-US AXXB calibration and imaging setup. Green arrows represent known transformations and red arrows represent calibration targets X_1 and X_2





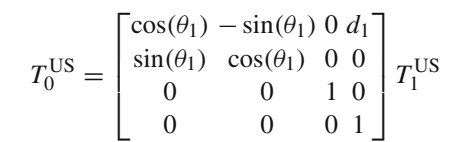
With the computed X_2 , we evaluate the result by comparing matrix AX against XB. The translational difference is 3.25 ± 1.79 mm (mean \pm std), and the rotational difference 0.68 ± 0.41 deg is computed by the taking the angular amplitude of the relative rotation $R = \text{rot}(AX) * \text{rot}(XB)^{\top}$.

After identifying X_1 , X_2 via TXp and AXXB calibration, the robot is programmed to scan the spine phantom within the AutoInFocus workspace.

Patch-based validation platform

To enhance portability and reduce cost, a wearable solution is preferred in point-of-care settings where lumbar punctures are usually performed. The result of the simulation (Sect. 3.1) and robot-based platform (Sect. 3.2.1) showed that a 2-DOF motion of the proposed workspace can sufficiently fulfill the coverage requirement. Therefore, we leveraged the reduction of DOF to simplify and miniaturize the robot-based platform into a small wearable device. We constructed a prototype (Fig. 4a) with a skin-contact footprint of approximately $100 \text{ mm} \times 50 \text{ mm}$. It is designed to be placed on the patient's back paramedianally to expose the needle access (Fig. 4b).

The 2-DOF motion is achieved with a parallel mechanism (Fig. 4c). The transducer is attached to a link that spans two parallel motor-driven linear stages. The link is connected to the first linear stage with a revolute joint and the second with a pin slot joint. A common motion of the two linear stages causes the transducer to translate and a differential motion causes the transducer to rotate. The kinematics is equivalent to a prismatic joint followed by a rotation joint (Fig. 4d). Let the two linear stage positions be q_1 and q_2 , respectively, and the minimum distance between the pins on the two linear stages be d_p . The forward kinematics from the base to the ultrasound frame (Fig. 4d) is



where $d_1 = q_1$ and $\theta_1 = \text{atan2}(d_p, q_2 - q_1)$. T_1^{US} is a constant dependent on the mounting position of the transducer.

In our prototype, the linear stages have 50 mm range of motion. In the central 26 mm of the linear motion, the pin slot joint rotates the transducer link up to 45 degrees in either direction. The maximum rotation decays toward the limits of the linear motion. The transducer is tilted 15 degrees toward the midline to further enlarge the useful workspace. We filled the gap between the transducer and the patient with a wedge-shaped elastic gel pad (Gelatin #4, Humimic Medical) to maintain acoustic coupling under the conical transducer surface trajectory.

We modified the transducer (ATL P7-4) to reduce its axial length and replaced the micro-coax cables with flat-flex cables to allow the transducer to freely translate and rotate inside the scanner housing.

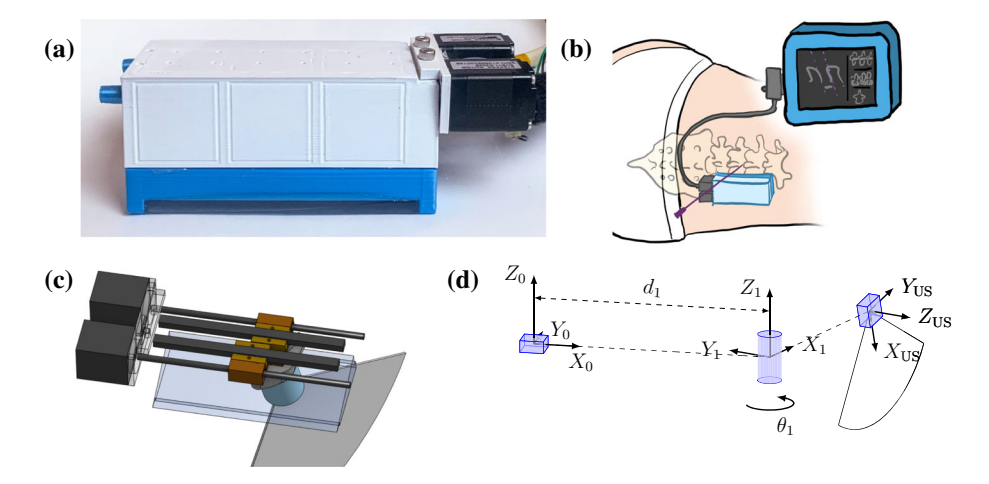
The pre-procedure volume is acquired in a shuttling motion. The transducer moves back and forth along the linear axis. At the end of each linear motion segment, the transducer rotates a small increment. We used 2 mm/s linear velocity and 5 degrees increment in the experiment, then selected 3 angles for further processing to match the robotic experiment. Each angle takes at most 25 s to acquire. The B-mode images were acquired on an ultrasound machine (Ultrasonix SonixTablet) at 30 fps.

Experiments and results

Simulation-based, robot-based, and patch-based AutoInFocus setups are independently evaluated to perform imaging experiments on the same spine phantom following the same workspace configuration.



Fig. 4 Patch-based validation platform. a Prototype scanner. b Proposed placement of the scanner. c The parallel actuation mechanism. d Equivalent kinematics



Quantitative visibility analysis with simulation

2D interspinous space visibility

In the current ultrasound-guided lumbar puncture workflow, sonographers typically image directly from the top of the vertebrae with a linear probe to visualize the interspinous space for locating the needle insertion point [5]. However, as shown in Fig. 5, only the top surfaces of the spinous process will be visualized due to the shadowing artifact, leaving an unclear definition of the interspinous space for needle insertion. Instead, we show that with AutoInFocus, this space can be better defined for identifying a needle insertion path in the 2D view

A simulated 6-cm linear probe is placed in the median sagittal plane in the simulator, and the AutoInFocus scanner is placed parallel to the side of the spine midline on the patient surface as shown in Fig. 6b. Then the crosssectional image Fig. 5b of the 3D reconstructed volume at the median sagittal plane is taken to compare with the 6 cm linear probe image shown in Fig. 5a. We empirically define the start and end points of the interspinous space boundary and delineate the visible boundaries from both images. Based on the number of effective boundary pixels, we show that the reconstructed AutoInFocus cross section has superior visibility of the interspinous space using an interspinous space visualization score, which is defined as the ratio of effective boundary pixel count between simulation and CT ground truth. Specifically, 69.46% (414/596 pixels) of the boundary is visualized in the AutoInFocus setup compared to 44.13% (263/596 pixels) using the traditional linear probe setup.

We also evaluate the imaging effectiveness with varying scanner placements and imaging depths, as shown in Table 1. In general, the AutoInFocus setup shows superior visualization capability than the 2D linear probe in every setting. Particularly, when placing the scanner at 4.7 cm lateral off-

set from the midline and imaging the bone at 4.3 cm depth, the AutoInFocus setup delivers the best interspinous process visibility (72.32%). However, although placing the scanner farther away from the midline may allow a larger window for needle insertion and operator motion, it can sacrifice the visibility of the top part of the spinous process when it is shallow.

3D spine model visibility

With the AutoInFocus setup, not only are the 2D interspinous space boundaries more clearly visible, but also it generates a better 3D representation of the spine model. We specifically compare using a single angle from the AutoInFocus workspace (Fig. 6a) representing a traditional wobbler 3D probe and the full AutoInFocus workspace with 9 angles (Fig. 6b). For each mesh triangle on the segmented spine model, we extract the nearby voxels in the reconstructed simulation volume and record the average voxel intensity. If the intensity is above a predefined threshold, the mesh triangle is determined to be visible. Figure 6c and d shows the surface visibility maps of Fig. 6a and b imaging setups, respectively.

Figure 6 shows that the full AutoInFocus workspace visually revealed a better 3D representation of the spine with more complete spine anatomy. The covered surface area is 63.35 cm² with single angle imaging and 158.77 cm² with AutoInFocus setup. For a total model surface area of 442.64 cm², AutoInFocus has increased the coverage ratio from 14.31% to 35.87%.

Qualitative visibility analysis with the robot-based and patch-based platforms

Phantom study with the robot-based platform

Using the calibrated robotic ultrasound system, we conducted phantom experiments to demonstrate the benefit of using the



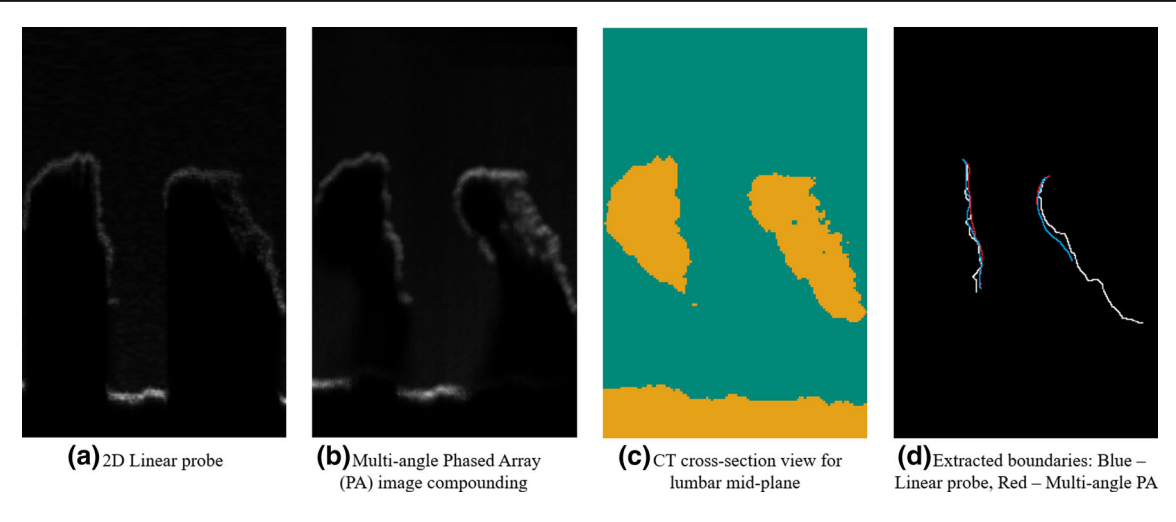


Fig. 5 Interspinous space midline plane visibility comparison between traditional 2D linear array and AutoInFocus setup

Table 1 Interspinous space visualization scores from varying scanner placement

Depth	Lateral offset from midline		
	2.5 cm (near)	3.6 cm	4.7 cm (far)
4.3 cm (deep)	0.6946	0.7114	0.7232
2.8 cm	0.6980	0.7198	0.6695
1.6 cm (shallow)	0.7181	0.6510	0.5105

Higher is better. The depth is measured from the skin surface to the top of the spinous process

AutoInFocus setup. For better demonstration, we select three angles {45°, 90°, 135°} from the AutoInFocus workspace, between the ultrasound image plane and the lumbar midline. For each angle, we sweep the transducer along the lumbar midline to acquire a set of parallel B-mode images, then reconstruct a volume.

The results are shown in Fig. 7. For each angle, we performed a 3D reconstruction and manually segmented the lumbar vertebrae in the 3D Slicer [22] platform following a sequence of thresholding, image closing and opening, and Gaussian/median smoothing. Then, we compounded all angles as shown in Fig. 7d and performed the same segmentation procedure to obtain the combined model in Fig. 7h. For each mesh triangle location on the combined model, we computed the average intensity of a $5 \times 5 \times 5$ voxels 3D block of all three volumes at the same mesh triangle center location. Then, we determined the volume with the highest average intensity at that location as the "dominant volume" and painted the mesh triangle with the corresponding color. The final result is shown in Fig. 7i, which demonstrates that AutoInFocus increases the chance of getting an echo from the complex spine anatomy with better-angled beams, as voxel intensity will be generally stronger with more appropriate specular reflection, thus providing superior visualization of the 3D interspinous space. In the end, note that although the scanner is placed on one side of the spine and only one upper quadrant of the anatomy can be visualized due to bone shadowing artifacts, it can meet the clinical requirement as long as the interspinous space is visualized.

Phantom study with the patch-based platform

We imaged the same spine phantom with the patch device, which has the same AutoInFocus workspace. The transducer suffers from image quality loss due to the modification process and only about 40 of the 64 elements are usable. Therefore, the image quality should not be compared with Fig. 7.

The reconstruction and visualization results from the patch-acquired volume data are shown in Fig. 8. In this experiment, the patch scanner ran 3 sweeps with different probe orientations, and the acquired sweeps were aligned in space for volume reconstruction. We manually registered the CT model of the spine phantom to the reconstructed ultrasound volume and showed the example 2D cross-sectional views from the US-CT overlay volume in Fig. 8a–c. In Fig. 8d, we can observe that a clear spinal shape can be visualized using maximum intensity projection. When overlaying the 3D visualization of the model, most of the high-intensity acoustic responses match the CT model surface as shown in Fig. 8, demonstrating the fidelity.

Discussion

Improved visibility of critical anatomical features. From both Figs. 5 and 6, we can observe that the vertebra shapes can be better revealed by the AutoInFocus setup. A clear definition of the key anatomy is crucial for many clinical applications



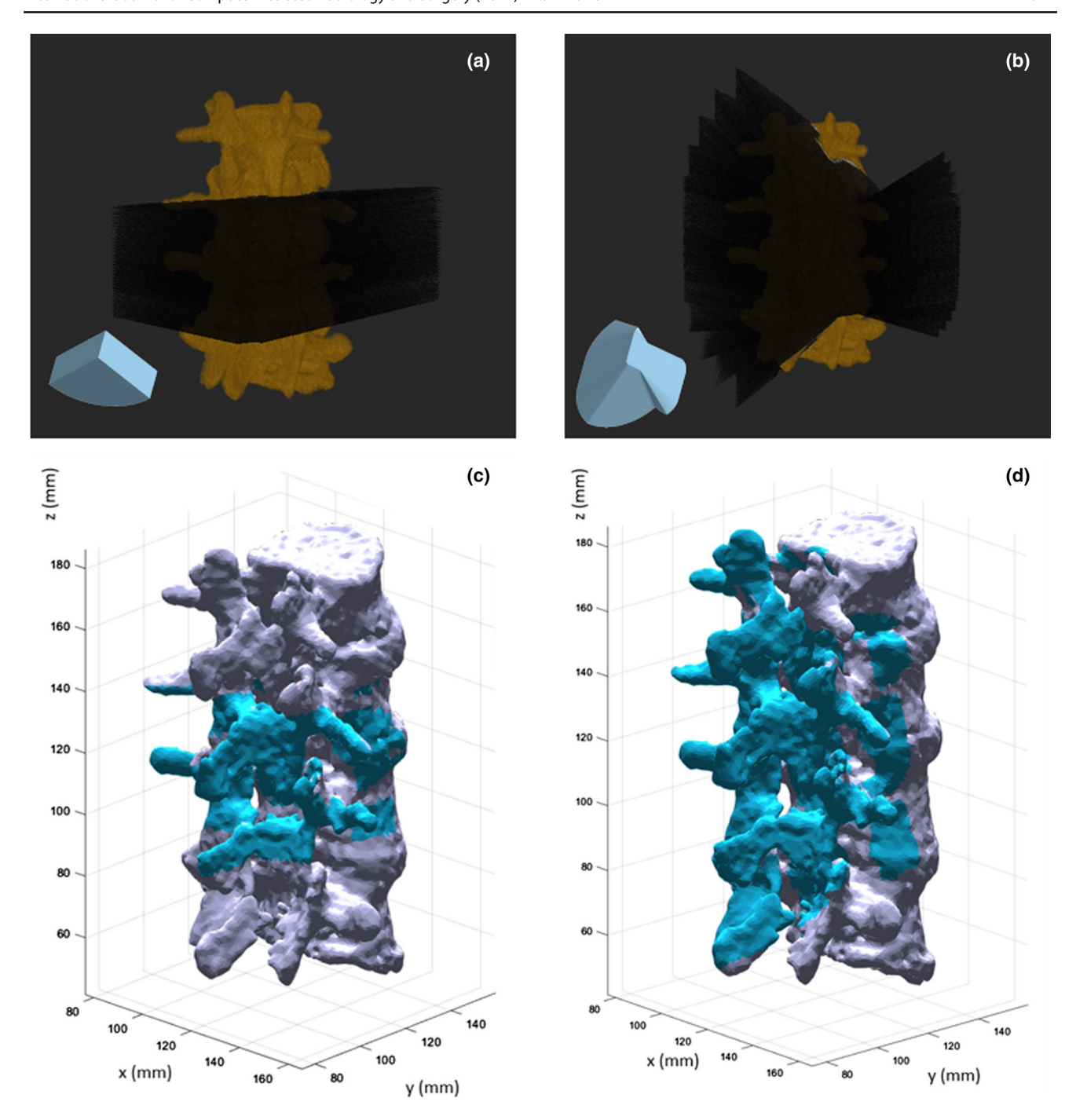


Fig. 6 3D anatomy coverage comparison. **a** Workspace with a single insonification angle. The inset is the 3D rendering of the workspace geometry (different view). **b** Workspace with 9 insonification angles.

c Surface visibility map of (a), where the blue mesh triangles represent that the nearby voxels have high response intensities in simulated ultrasound volume. **d** Surface visibility map of (b)

such as lumbar puncture, where the interspinous space needs to be defined for performing pre-procedure path planning and intra-procedure needle insertion guidance.

Enables imaging optimization with multi-insonification angles. As illustrated in Fig. 7, the quality of acoustic responses of the bone varies with the direction of insonifica-

tion. For example, when imaged from an optimal angle with minimal beam width artifact, the bone surface can be defined sharper. As a result, the AutoInFocus workspace includes a subset of high-quality beams, which enables quality-aware smart volume compounding methods.



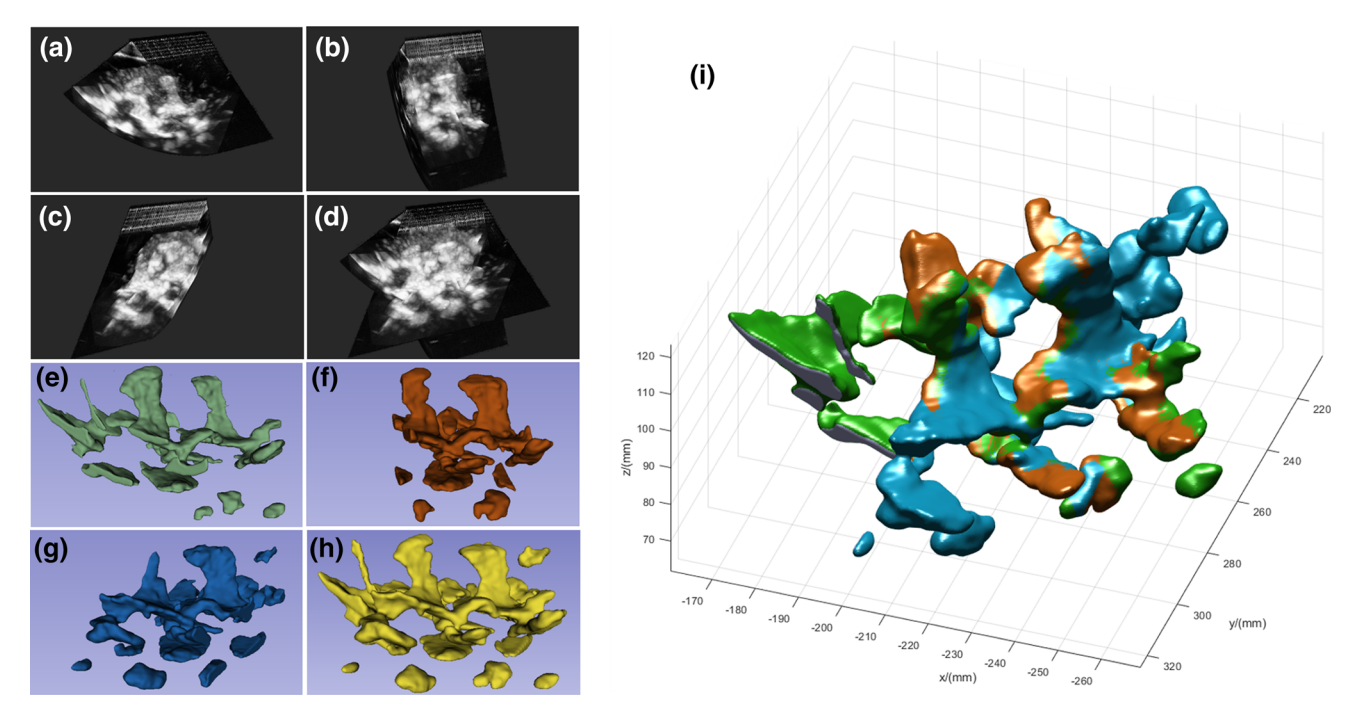
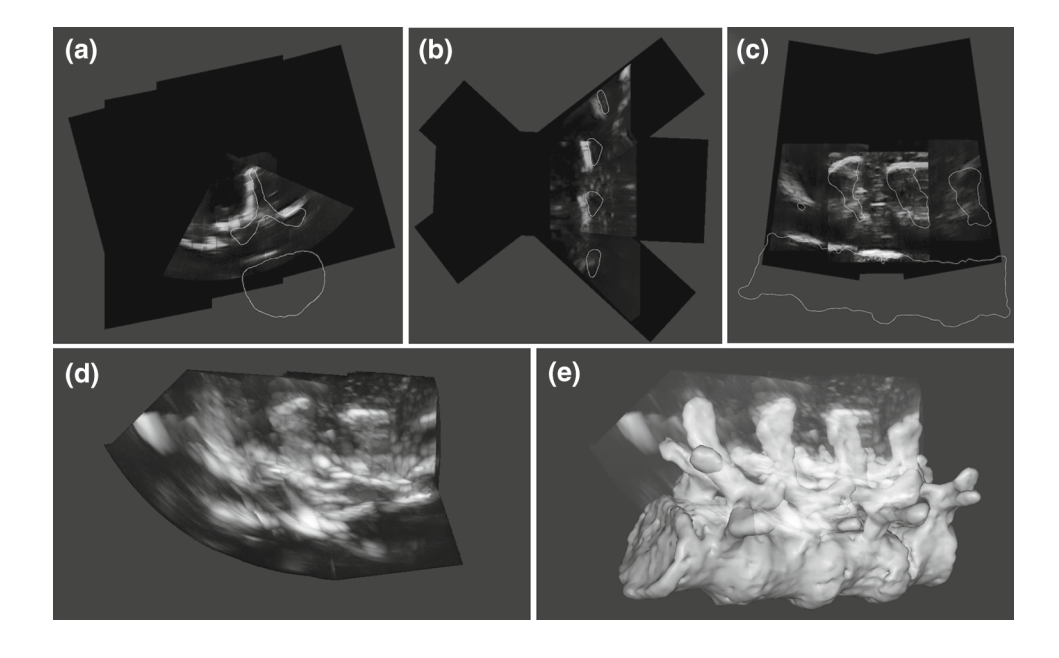


Fig. 7 Robotic scans of a lumbar phantom from 3 different angles in the AutoInFocus workspace. **a–c** Individual angle scans. **d** Compounded volume. **e–h** Manually segmented spine models corresponding to (a–d).

i The same model as in (h) but the mesh colors indicate the dominant contributing volume for each mesh triangle

Fig. 8 Patch device phantom scan. Three sweeps of data from the AutoInFocus workspace were selected for visualization. (a-c) The transverse (a), coronal (b), and sagittal (c) cross sections of the 3D-reconstructed ultrasound volume compared to the CT cross-sectional boundaries (white lines). (d) The 3D reconstructed patch ultrasound volume from three-angle sweeps. (e) 3D ultrasound reconstruction overlaid with the CT model



Tolerates non-optimal probe placement. Traditional ultrasound image guidance for spine interventions is unforgiving to probe placement due to shadowed anatomical landmarks [1]. This is especially problematic in hands-free applications because the probe placement cannot be manually readjusted during the procedure. Our design covers a large workspace with a small footprint, thus tolerating some placement errors and accommodating varying patient sizes as

shown in Table. 1. Figures 6 and 8 show that one good single probe placement could visualize three interspinous spaces with decent coverage in each. The size of the workspace is mostly limited by the length of the translational motion. It is virtually unlimited in the robot-based solution, but conforming to the surface geometry of the skin during the entire scan will require closed-loop force control. In the patch device solution, a long translational motion requires a long rigid



device, which can be unwieldy and unable to maintain acoustic coupling due to the same skin conformation problem.

Hands-free. Both the robot-based and patch-based realizations minimize the learning curve and disruption of the clinical workflow by allowing the physician to use both hands to manipulate the needle and not restricting the needle with a needle guide. In addition, the patch-based system enables the following workflow: (1) The patch shows real-time B-mode images in the transverse plane and guides the physician to place the patch on the patient. (2) The patch completes a full scan and displays a 3D volume and a sagittal view. (3) The physician plans a needle path in the volume and starts the needle insertion. (4) The transducer servos around the needle to provide real-time updates to the display.

Conclusion and future work

In this work, we have introduced a new imaging paradigm for spinal intervention guidance, and three evaluation platforms were developed. It is shown to improve the range and completeness of spine anatomy coverage in simulation. Two realizations of AutoInFocus have been presented with a robot-based setup and a miniaturized patch-based setup. Imaging experiments of these two systems have demonstrated the feasibility and superiority for imaging the challenging spine anatomy.

In future studies, we will scan *in vivo* animal tissue, which will enable us to develop algorithms for extracting spine bone surfaces by taking advantage of the multi-angle volumes. In addition, we will investigate increasing the frame rate via online insonification angle optimization that looks for the optimal subsets of volumes and ultimately integrate with the image processing, needle tracking, and augmented reality components to complete the clinical workflow and enable future clinical studies.

Acknowledgements We would like to acknowledge Dr. Pezhman Foroughi, Mr. Christopher Schlichter, Dr. Purnima Rajan, Dr. Alican Demir, and Dr. Ashraf Saad. Also, we would like to extend our acknowledgment to our sponsors and funding agencies: funding from National Science Foundation SCH:CAREER Grant No. 1653322, National Institute of Health 1R43EB031731, and Analog Devices Inc. fellowship.

Funding This study was funded by National Science Foundation SCH:CAREER Grant No. 1653322, National Institute of Health 1R43EB031731, and Analog Devices Inc. fellowship.

Declarations

Conflict of interest: Emad Boctor is a co-founder of and owns equity in Clear Guide Medical. The terms of this arrangement are being managed by the Johns Hopkins University in accordance with its conflict of

interest policies. Keshuai Xu, Baichuan Jiang, Abhay Moghekar, and Peter Kazanzides declare that they have no conflict of interest.

Ethical approval: This article does not contain any studies with human participants or animals performed by any of the authors.

Informed consent: This article does not contain patient data.

References

- Gueziri H-E, Santaguida C, Collins DL (2020) The state-of-theart in ultrasound-guided spine interventions. Med Image Anal 65:101769
- Hacihaliloglu I, Rasoulian A, Rohling RN, Abolmaesumi P (2013) Statistical shape model to 3D ultrasound registration for spine interventions using enhanced local phase features. Springer, pp 361–368
- Teng W-N, Tsou M-Y, Chang W-K, Ting C-K (2017) Eyes on the needle: identification and confirmation of the epidural space. Asian J Anesthesiol 55(2):30–34
- Zhang HK, Kim Y, Lin M, Paredes M, Kannan K, Moghekar A, Durr NJ, Boctor EM (2018) Toward dynamic lumbar puncture guidance using needle-based single-element ultrasound imaging. J Med Imaging 5(2):021224
- Soni NJ, Franco-Sadud R, Schnobrich D, Dancel R, Tierney DM, Salame G, Restrepo MI, McHardy P (2016) Ultrasound guidance for lumbar puncture. Neurol Clin Practice 6(4):358–368
- Peterson MA, Abele J (2005) Bedside ultrasound for difficult lumbar puncture. J Emerg Med 28(2):197–200
- Edwards C, Leira EC, Gonzalez-Alegre P (2015) Residency training: a failed lumbar puncture is more about obesity than lack of ability. Neurology 84(10):69–72
- Rosiak G, Lusakowska A, Milczarek K, Konecki D, Fraczek A, Rowinski O, Kostera-Pruszczyk A (2021) Ultra-low radiation dose protocol for CT-guided intrathecal nusinersen injections for patients with spinal muscular atrophy and severe scoliosis. Neuroradiology 63(4):539–545
- Seeberger MD, Kaufmann M, Staender S, Schneider M, Scheidegger D (1996) Repeated dural punctures increase the incidence of postdural puncture headache. Anesthesia and Analgesia 82(2):302–305
- Gorchynski J, Oman J, Newton T (2007) Interpretation of traumatic lumbar punctures in the setting of possible subarachnoid hemorrhage: Who can be safely discharged? California J Emerg Med 8(1):3
- Teele DW, Dashefsky B, Rakusan T, Klein JO (1981) Meningitis after lumbar puncture in children with bacteremia. New England J Med 305(18):1079–1081
- 12. Millington SJ, Restrepo MS, Koenig S (2018) Better with ultrasound: lumbar puncture. Chest 154(5):1223–1229
- Lee P-Y, Huang C-C, Chiang HK (2013) Implementation of a novel high frequency ultrasound device for guiding epidural anesthesiain vivo animal study. IEEE, pp 2049–2052
- Xu K, Kim Y, Boctor EM, Zhang HK (2019) Enabling low-cost point-of-care ultrasound imaging system using single element transducer and delta configuration actuator. Medical Imaging 2019: Image-Guided Procedures, Robotic Interventions, and Modeling, vol 10951. International Society for Optics and Photonics, p 109510
- Jensen JA (1996) Field, a program for simulating ultrasound systems, pp 351–353
- Treeby BE, Cox BT (2010) k-wave: Matlab toolbox for the simulation and reconstruction of photoacoustic wave fields. J Biomed Optic 15(2):021314



- Salehi M, Ahmadi S-A, Prevost R, Navab N, Wein W (2015) Patient-specific 3D ultrasound simulation based on convolutional ray-tracing and appearance optimization. Springer, pp 510–518
- Burger B, Bettinghausen S, Radle M, Hesser J (2012) Real-time GPU-based ultrasound simulation using deformable mesh models. IEEE Trans Med Imaging 32(3):609–618
- Guo X, Cheng A, Zhang HK, Kang H-J, Etienne-Cummings R, Boctor EM (2014) Active echo: a new paradigm for ultrasound calibration. Springer, pp 397–404
- Ackerman MK, Cheng A, Boctor E, Chirikjian G (2014) Online ultrasound sensor calibration using gradient descent on the Euclidean group. IEEE, pp 4900–4905
- Park FC, Martin BJ (1994) Robot sensor calibration: solving AX=XB on the Euclidean group. IEEE Trans Robot Autom 10(5):717-721
- 22. Fedorov A, Beichel R, Kalpathy-Cramer J, Finet J, Fillion-Robin J-C, Pujol S, Bauer C, Jennings D, Fennessy F, Sonka M, Buatti J, Aylward S, Miller JV, Pieper S, Kikinis R (2012) 3D Slicer as an image computing platform for the quantitative imaging network. Magnetic Resonance Imaging 30(9):1323–1341

Publisher's Note Springer Nature remains neutral with regard to jurisdictional claims in published maps and institutional affiliations.

